Transit Met Chem (2017) 42:181–191
DOI 10.1007/s11243-017-0123-2

Syntheses and photocatalytic performances of four coordination complexes constructed from 1,10-phenanthroline and polycarboxylic acids

Xiao-Xu Song[1,2] · Chong-Chen Wang[1,2] · Xue-Yan Xu[1] · Huan-Ping Jing[1] · Peng Wang[1] · Shi-Jie Gao[1]

Received: 22 October 2016 / Accepted: 27 January 2017 / Published online: 4 February 2017
© Springer International Publishing Switzerland 2017

Abstract Four coordination complexes of copper(II) and iron(II), namely $[CuCl(phen)_2](5\text{-}NO_2\text{-}Hipa)\cdot 2H_2O$ (**BUC-10**), $[Cu(phen)(3,4\text{-}H_2dczpb)(H_2O)]\cdot H_2O$ (**BUC-11**), $[Fe(phen)(L)(H_2O)]_2$ (**BUC-12**), and $[Fe(phen)_3](3,4\text{-}H_3dczpb)_2\cdot 0.6H_2O$ (**BUC-13**) (phen = 1,10-phenanthroline; $5\text{-}NO_2\text{-}H_2ipa$ = 5-nitroisophthalic acid; $3,4\text{-}H_4dczpb$ = 3,4-dicarboxyl-(3′,4′-dicarboxylazophenyl) benzene; L = 6, 12-dihydroxy-1,2,6,12-tetrahydroindazolo[2,1-a]indazole-1, 7-dicarboxylic acid), have been synthesized under hydrother mal conditions. All four complexes were characterized by single-crystal X-ray diffraction, FTIR, elemental analysis and UV–Vis diffuse reflection spectroscopy. The photocatalytic performances of the complexes for decomposition of methylene blue under UV irradiation were also investigated.

Introduction

Considering their diverse and easily tailored structures, along with their various potential applications [1] in catalysis [2–5], separation [6], gas storage [7], carbon dioxide capture [8] and so on [9], coordination compounds as examples of functional organic–inorganic hybrid porous materials have gained increasing attention [9–11]. Recently, coordination complexes and their derivatives have been found to have potential applications as heterogeneous photocatalysts, due to the presence of catalytically active metal sites and/or functional organic linkers as well as easily tailorable physical and chemical functionality of the catalytic moieties [12]. Hence, much attention has been paid to the catalytic degradation of organic pollutants [13–15], CO_2 reduction [15, 16], Cr(VI) reduction [15, 17, 18] and water splitting [19–21] using coordination compounds as photocatalysts.

The structures of such coordination compounds are primarily influenced by factors including the choice of metal centers, organic linkers, solvents and counterions [9, 14, 22]; variation of the organic linker can lead to very different structures [23, 24]. As typical ligands, multi-carboxylate linkers are of immense interest in the construction of versatile coordination architectures, due to the fact that they can link metal centers together and/or compensate the positive charge of the metal ions [24–26]. In order to investigate the influence of different organic linkers on the structures and properties of coordination compounds, three different multi-carboxylic acid ligands, namely 5-nitroisophthalic acid ($5\text{-}NO_2\text{-}H_2ipa$); 3,4-dicarboxyl-(3′,4′-dicarboxylazophenyl) benzene ($3,4\text{-}H_4dczpb$); and 6,12-dihydroxy-1,2,6,12-tetrahydroindazolo[2,1-a]indazole-1,7-dicarboxylic acid (L), as shown in Scheme 1, along with 1,10-phenanthroline (phen) as chelating ligand, were utilized to build four coordination compounds with different structures, i.e., $[CuCl(phen)_2](5\text{-}NO_2\text{-}Hipa)\cdot 2H_2O$ (**BUC-10**), $[Cu(phen)(3,4\text{-}H_2dczpb)(H_2O)]\cdot H_2O$ (**BUC-11**), $[Fe(phen)(L)(H_2O)]_2$ (**BUC-12**), and $[Fe(phen)_3](3,4\text{-}H_3dczpb)_2\cdot 0.6H_2O$ (**BUC-13**). The crystal structures of the complexes, as well as their optical gaps and photocatalytic activities toward degradation of methylene blue (MB),

Electronic supplementary material The online version of this article (doi:10.1007/s11243-017-0123-2) contains supplementary material, which is available to authorized users.

✉ Chong-Chen Wang
chongchenwang@126.com

[1] Beijing Key Laboratory of Functional Materials for Building Structure and Environment Remediation, Beijing University of Civil Engineering and Architecture, Beijing 100044, China

[2] Key Laboratory of Urban Stormwater System and Water Environment (Ministry of Education), Beijing University of Civil Engineering and Architecture, Beijing 100044, China

have been investigated. Factors influencing the activity and stability of **BUC-12** in photocatalytic reactions were also studied.

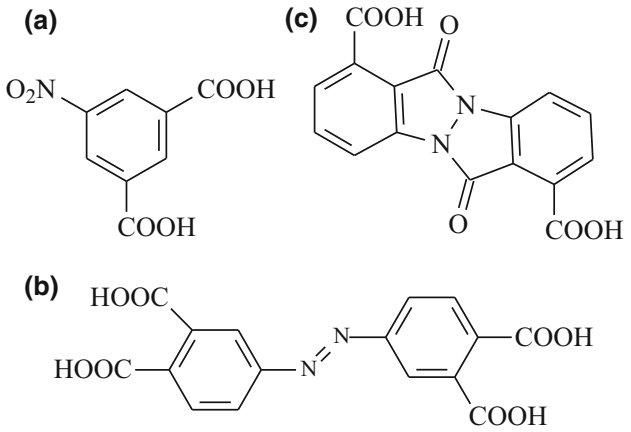

Scheme 1 Structural formulae of 5-NO_2-ipa (**a**), 3,4-H_4dczpb (**b**) and L (**c**)

Experimental

Materials and methods

All chemicals were commercially available reagent grade and used without further purification. C, N, H elemental analyses were obtained using an Elementar Vario EL-III instrument. The Fourier transform infrared (FTIR) spectra were recorded on a Nicolet-6700 spectrophotometer in the region (4000–400 cm^{-1}). UV–Vis diffuse reflection spectra of solid samples were measured from 200 to 800 nm on a PerkinElmer Lamda 650S spectrophotometer, in which $BaSO_4$ was used as the reference with 100% reflectance.

Synthesis of BUC-10

A mixture of $CuCl_2{\cdot}2H_2O$ (0.3 mmol, 0.0511 g), 5-NO_2-H_2ipa (0.3 mmol, 0.0663 g) and 1,10-phen (0.6 mmol, 0.1189 g) in a mole ratio of 1:1:2 was sealed in a 25-mL Teflon-lined stainless steel Parr bomb containing deionized H_2O (20 mL). The mixture was heated at 160 °C for 72 h and then cooled to room temperature. Green rod-like crystals of $[CuCl(phen)_2](5\text{-}NO_2\text{-}Hipa){\cdot}2H_2O$ (**BUC-10**)

Table 1 Details of X-ray data collection and refinement for **BUC 10–13**

	BUC-10	BUC-11	BUC-12	BUC-13
Formula	$C_{32}H_{24}ClCuN_5O_8$	$C_{28}H_{20}CuN_4O_{10}$	$C_{56}H_{32}Fe_2N_8O_{14}$	$C_{68}H_{43.20}FeN_{10}O_{16.60}$
M	705.55	636.02	17152.60	1321.78
Crystal system	Triclinic	Orthorhombic	Triclinic	Monoclinic
Space group	Pī	Pbca	Pī	P2/c
a (Å)	10.4950(8)	7.1586(6)	10.3940(8)	13.4640(11)
b (Å)	12.1359(11)	19.9971(13)	11.1641(9)	13.6049(12)
c (Å)	12.5491(12)	35.102(2)	11.1769(11)	21.4661(18)
α (°)	72.7040(10)	90	114.035(2)	90
β (°)	84.978(2)	90	93.1880(10)	127.812(3)
γ (°)	77.9540(10)	90	90.7770(10)	90
V ($Å^3$)	1491.9(2)	5024.8(6)	1181.75(18)	3106.4(5)
Z	2	8	1	2
μ (Mo, Kα) (mm^{-1})	0.885	1.868	0.699	0.323
Total reflections	7444	10367	5695	15261
Unique	5134	4382	4014	5470
F(000)	722	2600	588	1360
Goodness of fit on F^2	1.110	1.024	1.068	1.010
R_{int}	0.0275	0.0611	0.0570	0.0699
*R*1	0.0572	0.0538	0.0864	0.0549
ω*R*2	0.1213	0.1155	0.2033	0.1030
*R*1 (all data)	0.1018	0.0898	0.1298	0.1257
ω*R*2 (all data)	0.1433	0.1382	0.2306	0.1235
Largest diff. Peak and hole (e/$Å^3$)	0.587, −0.666	0.345, −0.491	1.187, −0.982	0.452, −0.281

Table 2 Selected bond lengths and angles for **BUC 10-13** [Å and °]

BUC-10						
Bond lengths (Å)						
Cu(1)–N(3)	1.988(3)		Cu(1)–N(1)	1.999(3)	Cu(1)–N(4)	2.075(4)
Cu(1)–N(2)	2.173(4)		Cu(1)–Cl(1)	2.2810(15)		
Bond angles (°)						
N(3)–Cu(1)–N(1)		174.57(17)		N(3)–Cu(1)–N(4)	80.71(15)	
N(1)–Cu(1)–N(4)		97.60(14)		N(3)–Cu(1)–N(2)	96.02(15)	
N(1)–Cu(1)–N(2)		79.59(15)		N(4)–Cu(1)–N(2)	108.80(15)	
N(3)–Cu(1)–Cl(1)		94.99(12)		N(1)–Cu(1)–Cl(1)	89.66(12)	
N(4)–Cu(1)–Cl(1)		138.97(11)		N(2)–Cu(1)–Cl(1)	112.22(11)	
BUC-11						
Bond lengths (Å)						
Cu(1)–O(4)	1.930(3)		Cu(1)–O(5)	1.960(3)	Cu(1)–N(2)	2.004(3)
Cu(1)–N(1)	2.019(3)		Cu(1)–O(9)	2.278(3)		
Bond angles (°)						
O(4)–Cu(1)–O(5)		91.42(13)		O(4)–Cu(1)–N(2)	95.35(13)	
O(5)–Cu(1)–N(2)		169.88(13)		O(4)–Cu(1)–N(1)	175.96(14)	
O(5)–Cu(1)–N(1)		91.37(13)		N(2)–Cu(1)–N(1)	81.51(14)	
O(4)–Cu(1)–O(9)		77.53(13)		O(5)–Cu(1)–O(9)	88.05(13)	
N(2)–Cu(1)–O(9)		100.74(14)		N(1)–Cu(1)–O(9)	105.48(14)	
BUC-12						
Bond lengths (Å)						
Fe(1)–O(3)	2.023(4)		Fe(1)–O(7)	2.083(4)	Fe(1)–O(5)#1	2.145(4)
Fe(1)–N(4)	2.181(5)		Fe(1)–N(3)	2.205(5)	Fe(1)–O(1)	2.285(4)
Bond angles (°)						
O(3)–Fe(1)–O(7)		101.14(18)		O(3)–Fe(1)–O(5)#1	103.69(17)	
O(7)–Fe(1)–O(5)#1		87.02(16)		O(3)–Fe(1)–N(4)	153.02(19)	
O(7)–Fe(1)–N(4)		100.44(17)		O(5)#1–Fe(1)–N(4)	93.39(18)	
O(3)–Fe(1)–N(3)		90.50(17)		O(7)–Fe(1)–N(3)	86.32(17)	
O(5)#1–Fe(1)–N(3)		165.25(17)		N(4)–Fe(1)–N(3)	74.93(18)	
O(3)–Fe(1)–O(1)		82.97(16)		O(7)–Fe(1)–O(1)	163.70(15)	
O(5)#1–Fe(1)–O(1)		76.68(15)		N(4)–Fe(1)–O(1)	80.83(16)	
N(3)–Fe(1)–O(1)		109.54(15)				
Symmetry transformations used to generate equivalent atoms: #1 $-x + 1, -y + 1, -z + 1$						
BUC-13						
Bond lengths (Å)						
Fe(1)–N(2)#1	1.963(3)		Fe(1)–N(2)	1.963(3)	Fe(1)–N(3)	1.973(3)
Fe(1)–N(3)#1	1.973(3)		Fe(1)–N(1)	1.976(2)	Fe(1)–N(1)#1	1.976(2)
Bond angles (°)						
N(2)#1–Fe(1)–N(2)		92.92(14)		N(2)#1–Fe(1)–N(3)	92.44(10)	
N(2)–Fe(1)–N(3)		171.79(10)		N(2)#1–Fe(1)–N(3)#1	171.79(10)	
N(2)–Fe(1)–N(3)#1		92.44(10)		N(3)–Fe(1)–N(3)#1	82.93(16)	
N(2)#1–Fe(1)–N(1)		94.81(10)		N(2)–Fe(1)–N(1)	82.44(10)	
N(3)–Fe(1)–N(1)		90.92(10)		N(3)#1–Fe(1)–N(1)	92.05(9)	
N(2)#1–Fe(1)–N(1)#1		82.44(10)		N(2)–Fe(1)–N(1)#1	94.81(10)	
N(3)–Fe(1)–N(1)#1		92.05(9)		N(3)#1–Fe(1)–N(1)#1	90.92(10)	
N(1)–Fe(1)–N(1)#1		176.03(16)				
Symmetry transformations used to generate equivalent atoms: #1 $-x + 1, y, -z + 3/2$						

(yield 92% based on $CuCl_2{\cdot}2H_2O$) were isolated by filtration and washed with deionized water and ethanol. Anal. Calcd. for **BUC-10**, $C_{32}H_{24}ClCuN_5O_8$: C, 54.4; N, 9.9; H, 3.4. Found: C, 54.8; N, 10.0; H, 3.4%. IR (KBr)/cm^{-1}: 3578, 3108 m, 1953s, 1599, 1529, 1517, 1453 m, 1425 s, 1370, 1342 m, 1202, 1223, 1182, 1143, 1091, 1075w, 859, 782, 725, 646 m, 507, 428w.

Synthesis of BUC-11

Small black rod-like crystals of $[Cu(phen)(3,4\text{-}H_2dczpb)(H_2O)]{\cdot}H_2O$ (**BUC-11**) (yield 68% based on $CuCl_2{\cdot}2H_2O$) were synthesized from a mixture of $CuCl_2{\cdot}2H_2O$ (0.3 mmol, 0.0511 g), H_4dczpb (0.3 mmol, 0.1074 g) and 1,10-phen (0.6 mmol, 0.1189 g) in 1:1:2 M ratio under the same conditions as for **BUC-10**. Anal. Calcd. for **BUC-11**, $C_{28}H_{20}CuN_4O_{10}$: C, 52.8; N, 8.8; H, 3.1. Found: C, 52.9; N, 8.8; H, 3.2%. IR (KBr)/cm^{-1}: 3362, 3063, 2015, 1733, 1670, 1614, 1592, 1520, 1487 m, 1386 s, 1371, 1333, 1280 m, 1060w, 854, 802, 723 m, 673w.

Synthesis of BUC-12

Black rod-like crystals of $[Fe(phen)(L)(H_2O)]_2$ (**BUC-12**) (yield 92% based on $FeSO_4{\cdot}7H_2O$) were synthesized from a mixture of $FeSO_4{\cdot}7H_2O$ (0.3 mmol, 0.0834 g), L (0.3 mmol, 0.1074 g) and 1,10-phen (0.6 mmol, 0.1189 g) in 1:1:2 M ratio under the same conditions as for **BUC-10**. Anal. Calcd. for **BUC-12**, $C_{56}H_{32}Fe_2N_8O_{14}$: C, 58.3; N, 9.7; H, 2.8. Found: C, 58.4; N, 9.7; H, 2.9%. IR (KBr)/cm^{-1}: 2925, 1717, 1676, 1601 m, 1426 s, 1387, 1360, 1300 m, 1151, 1099w, 920 m, 880, 843w, 817, 771, 747 m, 657, 596w.

Synthesis of BUC-13

Red block-like crystals of $[Fe(phen)_3](3,4\text{-}H_3dczpb)_2{\cdot}0.6H_2O$ (**BUC-13**) (yield 90% based on $FeSO_4{\cdot}7H_2O$) were synthesized from a mixture of $FeSO_4{\cdot}7H_2O$ (0.3 mmol, 0.0834 g), 3,4-H_4dczpb (0.3 mmol, 0.1074 g) and 1,10-phen (0.6 mmol, 0.1189 g) in 1:1:2 M ratio under the same conditions as for **BUC-10**. Anal. Calcd. for **BUC-13**, $C_{68}H_{43.20}FeN_{10}O_{16.60}$: C, 62.3; N, 10.7; H, 3.2. Found: C, 62.8; N, 10.8; H, 3.4%. IR (KBr)/cm^{-1}: 3417, 3061, 1579, 1517, 1426 s, 1355, 1263 m, 1204, 1061, 847w, 775, 724 m, 656, 531w.

X-ray crystallography

X-ray single-crystal data collections for the complexes were performed with a Bruker Smart 1000 CCD area detector diffractometer with graphite-monochromatized MoKα radiation ($\lambda = 0.71073$ Å) using $\varphi - \omega$ mode at 293(2) K. The SMART software package [27] was used for data collection and SAINT software [28] for data extraction. Empirical absorption corrections were performed with the SADABS program [29]. The structures were solved by direct methods (SHELXS-97) [30] and refined by full-matrix-least squares techniques on F^2 with anisotropic thermal parameters for all non-hydrogen atoms (SHELXL-97) [30]. The hydrogen atoms of the organic ligands were added according to theoretical models, and those of water molecules were found by difference Fourier maps. All structural calculations were carried out using the SHELX-97 program package [30]. Crystallographic data and structural refinements for **BUC 10–13** are summarized in Table 1. Selected bond lengths and angles are listed in Table 2.

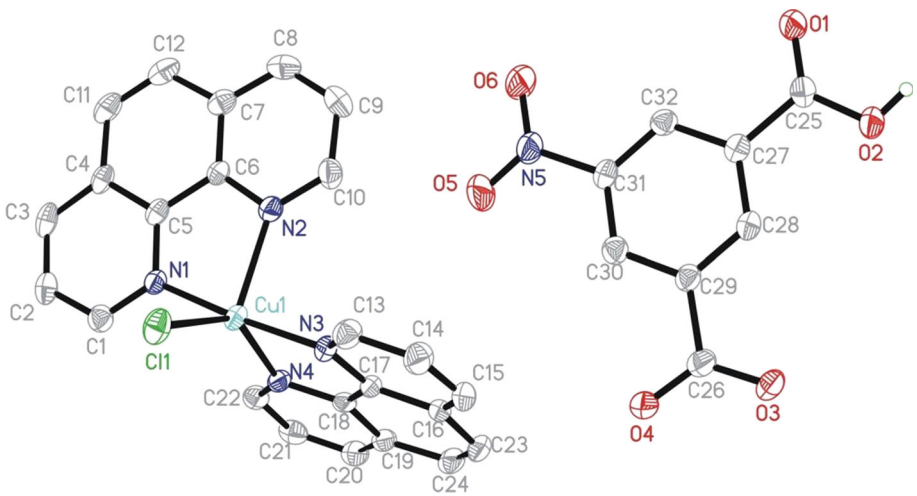

Fig. 1 ORTEP drawing of **BUC-10** showing the Cu(II) coordination environment with thermal ellipsoids at 30% probability (all hydrogen atoms attached on carbon atoms, oxygen atoms and the corresponding hydrogen atoms of lattice water molecules are omitted for clarity)

Table 3 Hydrogen bonds for **BUC 10–13** [Å and °]

D–H	d(D–H)	d(H..A)	<DHA	d(D..A)	A
BUC-10					
O2–H2	0.820	1.739	160.34	2.526	O7 [x, $y-1$, z]
O7–H7C	0.850	1.868	176.12	2.717	O8 [x, $y+1$, z − 1]
O7–H7D	0.850	1.815	175.68	2.663	O3 [−x, $-y+1$, −z + 1]
O8–H8C	0.850	1.797	173.24	2.643	O4
O8–H8D	0.850	2.574	174.60	3.422	Cl1 [$x-1$, y, z]
BUC-11					
O1–H1	0.820	1.743	176.75	2.562	O10
O8–H8	0.820	1.922	160.62	2.710	O2 [$x+1/2$, $-y+3/2$, $-z+1$]
O9–H9C	0.850	1.872	161.67	2.692	O3 [$x+1$, y, z]
O9–H9D	0.850	2.351	162.96	3.174	N3 [$x+1/2$, $-y+3/2$, $-z+1$]
O10–H10C	0.850	2.036	167.38	2.871	O5 [$-x+3/2$, $y-1/2$, z]
O10–H10D	0.850	1.944	167.17	2.779	O6 [$-x+1/2$, $y-1/2$, z]
BUC-12					
O7–H7C	0.850	1.886	162.64	2.709	O4 [$-x$, $-y+2$, $-z+1$]
O7–H7D	0.850	1.800	162.75	2.624	O6 [$-x+1$, $-y+1$, $-z+1$]
BUC-13					
O2–H2	0.820	1.560	171.54	2.374	O3
O5–H5	0.820	1.800	177.53	2.620	O4 [x, $-y+1$, $z+1/2$]
O8–H8	0.820	1.828	155.84	2.598	O1 [x, $-y+2$, $z+1/2$]

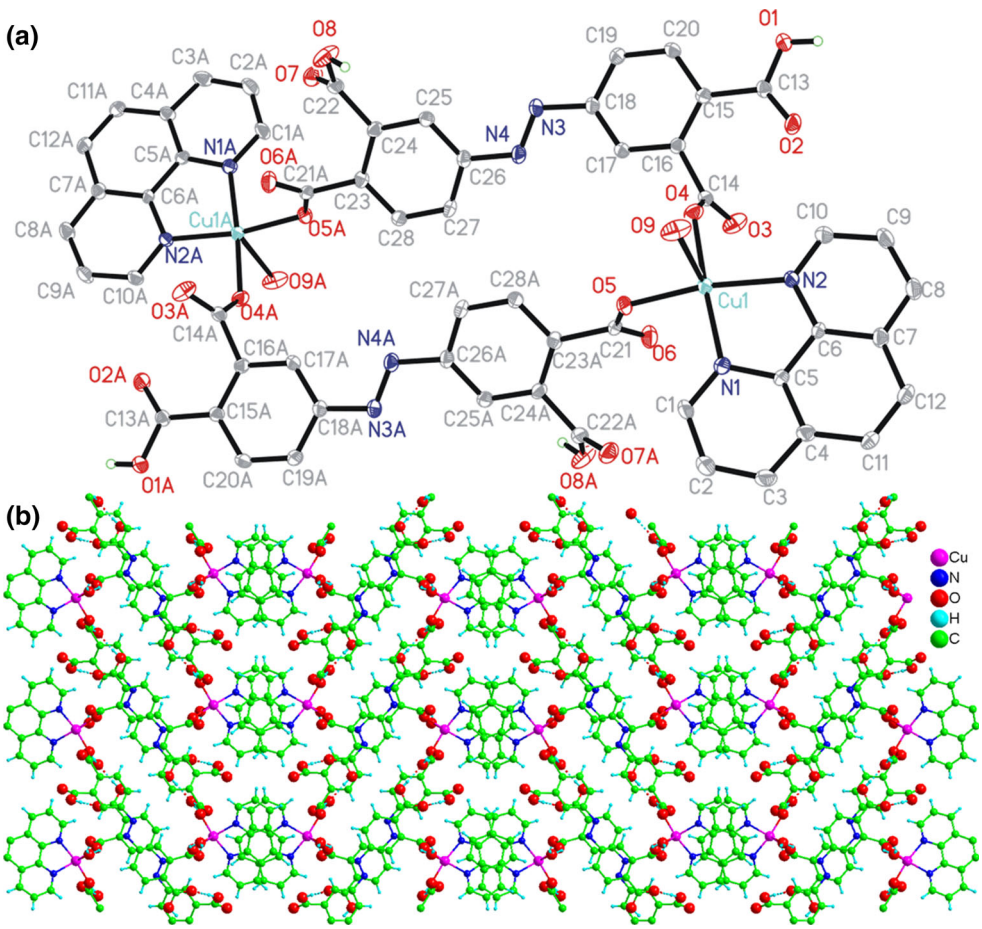

Fig. 2 **a** ORTEP drawing of **BUC-11** showing the Cu(II) coordination environment with thermal ellipsoids at 30% probability (all hydrogen atoms attached on carbon atoms, oxygen atoms and the corresponding hydrogen atoms of lattice water molecules are omitted for clarity). Symmetry code: **a** $-x+1$, $-y+2$, $-z+1$ and **b** Two-dimensional supramolecular layer structure of **BUC-11** formed by hydrogen-bonding interactions

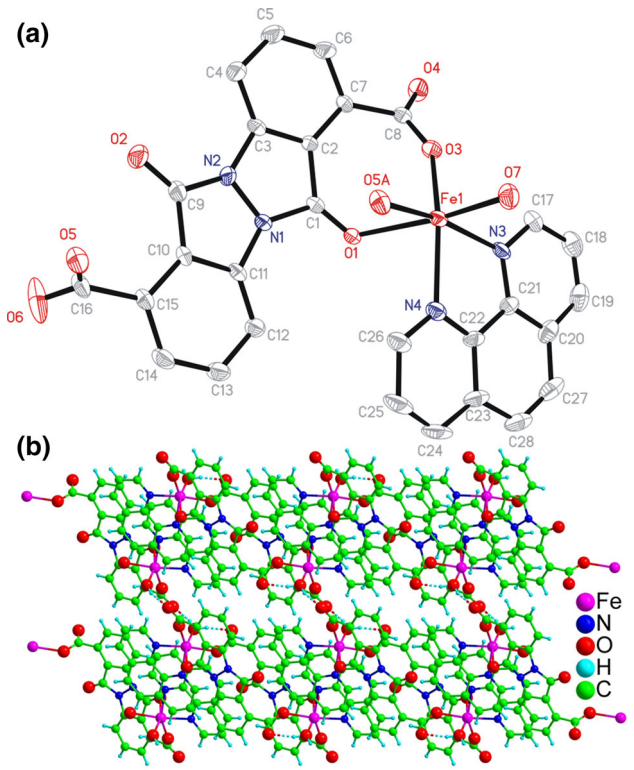

Fig. 3 **a** ORTEP drawing of **BUC-12** showing the Fe(II) coordination environment with thermal ellipsoids at 30% probability (all hydrogen atoms attached on carbon atoms, oxygen atoms and the corresponding hydrogen atoms of lattice water molecules are omitted for clarity). Symmetry code: **a** $-x + 1, -y + 1, -z + 1$ and **b** The packing structure of **BUC-12** viewed along the *c* axis

Photocatalytic degradation of MB

The activities of **BUC 10–13** as photocatalysts were evaluated using MB as a model organic pollutant at room temperature and under UV light irradiation in a photocatalytic assessment system (Beijing Aulight Co. Ltd.). The distance between the light source and the beaker containing the reaction mixture was fixed at 5 cm. The powdered photocatalyst, with a particle size less than 147 μm, was added to 200 mL of MB (10 mg/L) aqueous solution in a 300-mL beaker. Prior to UV irradiation, the suspension was magnetically stirred in the dark for 120 min to ensure the adsorption/desorption equilibrium. During the photocatalytic degradation, stirring was maintained to keep the mixture fully in suspension. One milliliter aliquots were extracted at regular time intervals using a 0.45-μm syringe filter (Shanghai Troody) for analysis. The solution was analyzed on a Laspec Alpha-1860 spectrometer over the range of 400–800 nm in a spectrometric quartz cell with 1 cm path length. The remaining MB concentration was determined at 664 nm.

In order to investigate the effect of pH on the photocatalytic MB degradation, the initial pH values of the 10 mg/L MB solution were adjusted to 2.0, 4.0, 6.0, 8.0 and 10.0, using HCl and NaOH solutions of suitable concentrations (50 mg of **BUC-12** was added to 200 mL of MB solution). In order to study the effect of salts, on the photocatalytic performance of **BUC-12**, tap water was used as a solvent containing sodium (18.42 mg/L), calcium (70.05 mg/L), magnesium (30.59 mg/L) and chloride (0.1 mg/L). The total dissolved solids content of the tap water was 452 mg/L.

Results and discussion

All of these coordination compounds were stable under air and insoluble in water and common organic solvents, including ethanol, methylbenzene, chloroform, ether, DMSO and DMF.

Structure of BUC-10

$[CuCl(phen)_2](5\text{-}NO_2\text{-}Hipa)\cdot 2H_2O$ (**BUC-10**) was synthesized under hydrothermal conditions. Although the crystal structure of BUC-10 has been previously reported by Xiao and coworkers [32], the current refinement was of better quality; the values of $R_{gt}(F)$ and $\omega R_{ref}(F^2)$ of **BUC-10** in the present work were 0.0572 and 0.1213, respectively, compared to those from the previously study ($R_{gt}(F) = 0.103$, $\omega R_{ref}(F^2) = 0.204$ [32]). The crystal structure analysis reveals that it is built up of discrete $[CuCl(phen)_2]$ units, partly deprotonated $5\text{-}NO_2\text{-}Hipa^-$ anions and two lattice water molecules. The Cu(II) center, in a distorted trigonal pyramidal geometry, is five-coordinated by four nitrogen atoms from two phen ligands and one chloride, such that N1, N2, N3 and N4 occupy the equatorial plane, and chloride occupies the vertex, as depicted in Fig. 1. The Cu–N bond distances range from 1.988(3) to 2.173(4) Å, and the Cu–Cl bond length is 2.2810(15) Å; these values are comparable with those typically found in similar coordination compounds [31]. In the equatorial plane, the N1–Cu1–N3 and N2–Cu1–N4 bond angles are 174.57(17)° and 108.80(15)°, respectively, showing that the copper's coordination sphere is severely distorted. In the crystal, a 3D supramolecular framework is assembled via abundant hydrogen-bonding interactions, as documented in Fig. S1(ESI) and Table 3.

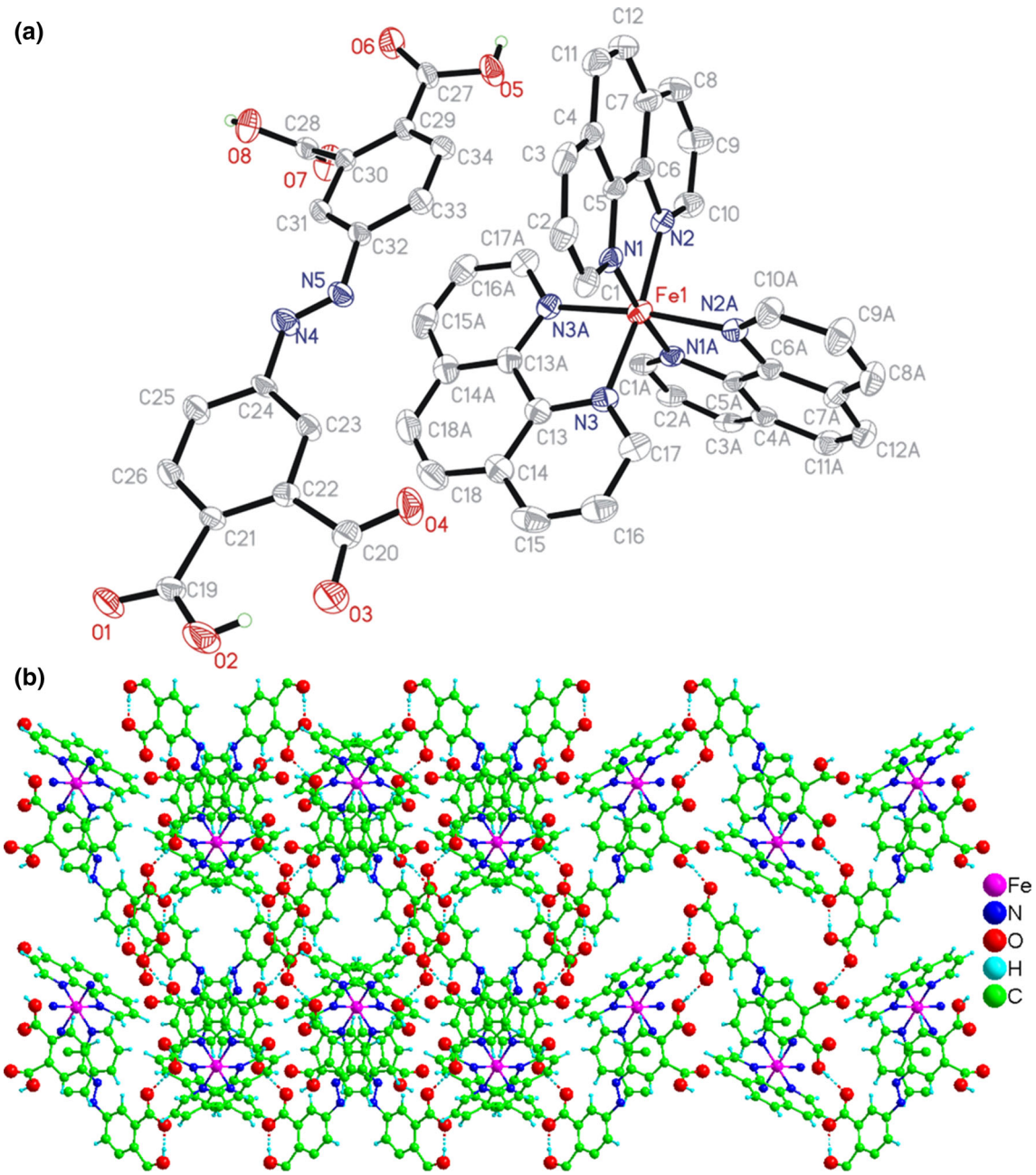

Fig. 4 **a** ORTEP drawing of **BUC-13** showing the Fe(II) coordination environment with thermal ellipsoids at 30% probability (all hydrogen atoms attached on carbon atoms, oxygen atoms and the corresponding hydrogen atoms of lattice water molecules are omitted for clarity). Symmetry code: **a** $-x + 1, y, -z + 3/2$. **b** 3D framework of **BUC-13** viewed along the *a* axis

Structure of BUC-11

In [Cu(phen)(3,4-H_2dczpb)(H_2O)]·H_2O (**BUC-11**), the Cu(II) center has a square-pyramidal geometry, being coordinated by N1 and N2 from a phen ligand, O4 and O5 from two different 3,4-H_2dczpb^{2-} ligands, plus atom O9 from a water ligand, as shown in Fig. 2a. The partly deprotonated 3,4-H_2dczpb^{2-} ligands adopt a bis-monodentate mode to link two [Cu(phen)(H_2O)]$^{2+}$ units into an approximately rectangular molecular box, as illustrated in Fig. 2a. These [Cu_2(phen)$_2$(3,4-H_2dczpb)$_2$(H_2O)$_2$] molecular boxes are further joined into a two-dimensional supramolecular layer structure in the *ab*-plane with the help of hydrogen-bonding interactions, as detailed in Fig. 2b and Table 3.

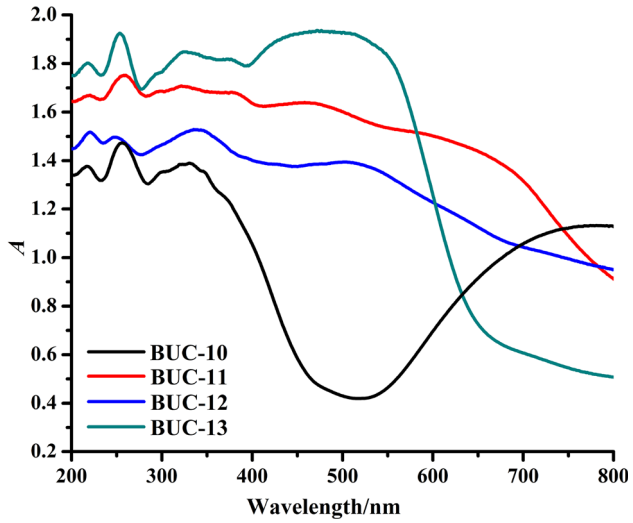

Fig. 5 UV–Vis diffuse reflectance spectra of **BUC 10–13**

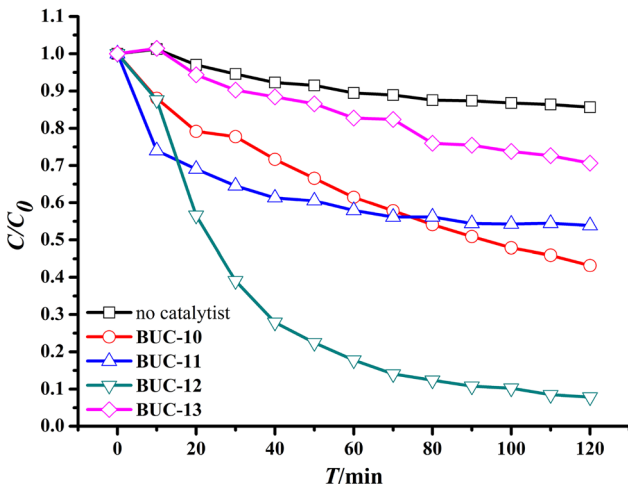

Fig. 6 Plots of concentration versus irradiation time for MB under irradiation with Hg lamp light using **BUC 10–13** as photocatalysts, and the control experiment without any photocatalyst

Structure of BUC-12

Similar to the structure of **BUC-11**, $[Fe(phen)(L)(H_2O)]_2$ **(BUC-12)** is based on a $[Fe(phen)(L)(H_2O)]_2$ molecular box, in which Fe(II) is six-coordinated in a distorted octahedral geometry provided by N3 and N4 from a phen ligand, O1 and O3 oxygen atoms from carboxylate and carbonyl groups from the same L ligand, O5A oxygen atom from another L ligand and O7 from a water ligand, as illustrated in Fig. 3a. In **BUC-12**, the completely deprotonated L ligand coordinates via a single O atom from its COO^- group plus chelating O atoms from both COO^- and OH^- groups to link Fe(II) centers. The $[Fe(phen)(L)(H_2O)]_2$ molecular boxes are linked into a chain-like structure via hydrogen-bonding interactions, as detailed in Fig. 3b and Table 3.

Structure of BUC-13

The structure of **BUC-13** ($[Fe(phen)_3](3,4\text{-}H_3dczpb)_2 \cdot 0.6H_2O$) consists of discrete $[Fe(phen)_3]^{2+}$ units, partly deprotonated 3,4-H_3dczpb^- anions and lattice water molecules. The Fe(II) center is in a distorted octahedral geometry provided by six nitrogen atoms from three phen ligands, as illustrated in Fig. 4a. The cationic charge of $[Fe(phen)_3]^{2+}$ is balanced by two 3,4-H_3dczpb^- anions. These partly deprotonated 3,4-H_3dczpb^- anions are assembled into sheets via hydrogen-bonding interactions (as listed in Fig. 4b; Table 3) and further connected by cationic $[Fe(phen)_3]^{2+}$ moieties into a 3D supramolecular structure via electrostatic and weak intermolecular interactions.

Optical and catalytic properties

In order to investigate the optical properties of **BUC 10–13**, their UV–Vis adsorption spectra for powdered samples were recorded at room temperature [33]. As shown in Fig. 5, these coordination polymers showed an adsorption peak in the range 250–400 nm, indicative of their selective absorptions in the ultraviolet region.

The photocatalytic performances of **BUC 10–13** for the decomposition of MB were assessed under UV irradiation. Control experiments on MB degradation without any catalyst under identical conditions were also carried out. In order to confirm the powder purity of **BUC-12** used in this experiment, powder X-ray diffraction was conducted. The powder X-ray pattern matched well with that simulated from the X-ray single-crystal diffraction data, as shown in Fig. 8, confirming the phase purity of bulk samples of **BUC-12**. The slight differences in intensities may be assigned to the preferred orientation of the crystalline powder samples [34]. The photocatalytic performances were monitored by measuring the maximum absorbance intensity at 664 nm, in order to determine the residual MB concentration. The degradation efficiencies of MB in the presence of **BUC 10–13** after prior adsorption equilibrium in the dark are shown in Fig. 6. All quantitative data for degradation efficiencies are average values from three parallel experiments. It can be seen that the degradation efficiency of MB increased from 14.4% (control experiment) to 57.8, 46.1, 92.1 and 29.3%, respectively, with **BUC-10**, **BUC-11**, **BUC-12** and **BUC-13** as photocatalysts for a runtime of 120 min. All of these photocatalytic degradation reactions followed a pseudo-first-order kinetic model. Thus, plots of $-\ln(C/C_0)$ versus reaction time were linear, giving R^2 values of 0.989, 0.698, 0.946 and 0.976, respectively. The pseudo-first-order rate constants (k) for the photocatalytic degradation of MB with **BUC-10**, **BUC-11**, **BUC-12** and **BUC-13** as photocatalysts were 0.0067,

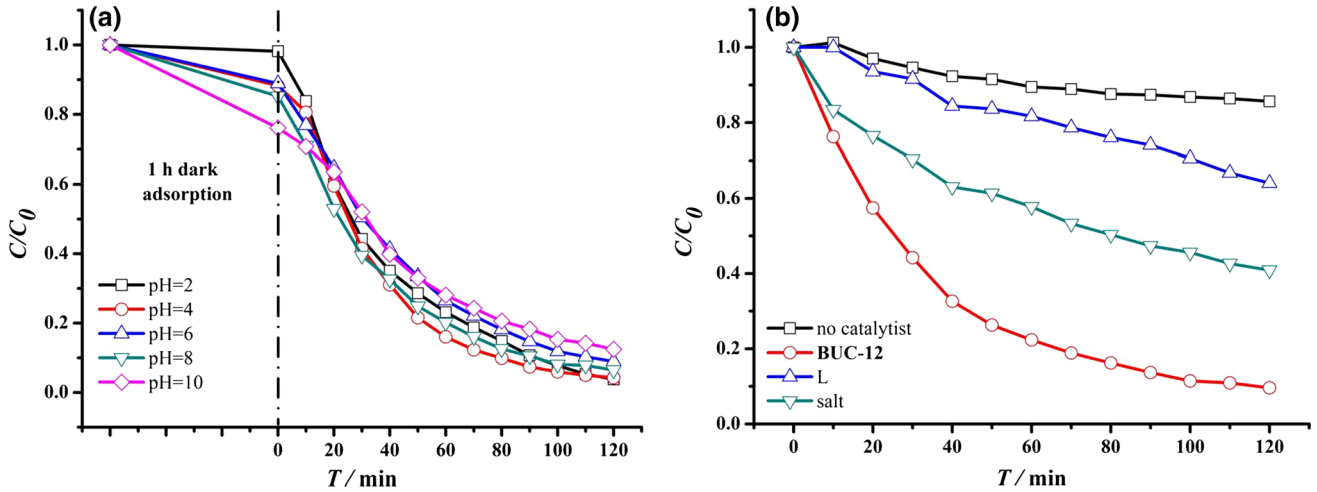

Fig. 7 **a** Effect of initial pH on the degradation of MB under UV irradiation using **BUC-12** as photocatalyst. **b** The effect of salts and ligands on the degradation of MB

Table 4 Effect of recycling **BUC-12** in the degradation of MB (10 mg/L)

Circulating runs	First run	Second run	Third run	Fourth run	Fifth run
Removal percentage (%)	96.1	95.9	95.4	95.4	95.1

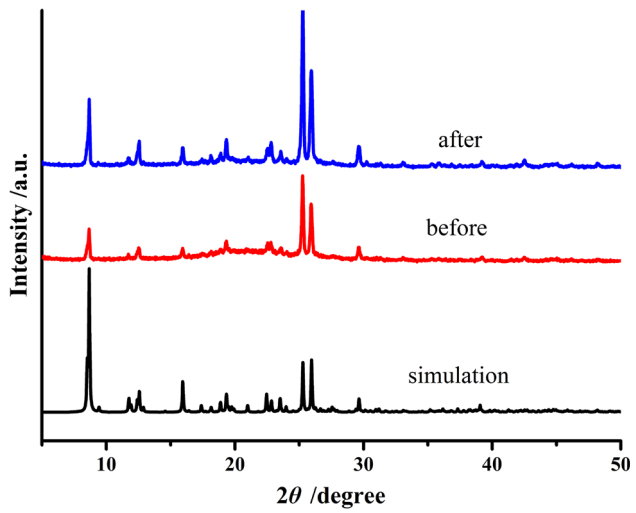

Fig. 8 PXRD patterns of **BUC-12** before and after photocatalytic reaction and the simulated XRD pattern from the single-crystal structure

0.0038, 0.0218 and 0.0031 min^{-1}, respectively. The noticeable differences in their photocatalytic performances might arise from the structures of these four coordination compounds, especially the role of the polycarboxylic acids. The 5-NO_2-$Hipa^-$ and 3,4-H_3dczpb^- in **BUC-10** and **BUC-13** are discrete anions and uncoordinated to the metal, whereas the 3,4-H_2dczpb^{2-} ligand in **BUC-11** is partly coordinated to the metal, with two COOH groups being undeprotonated. However, the L ligand in **BUC-12** is completely coordinated to the Fe^{2+} center. With this in mind, we propose that the uncoordinated COOH groups might capture ·OH radicals, affecting the catalysis. Further research will be required in order to clarify the relationship between the photocatalytic performances of these complexes and their structures.

The pH of the solution is another important parameter, which can influence photocatalytic degradation reactions [35]. Thus, the effect of initial pH on the degradation efficiency of MB using **BUC-12** as catalyst was tested. The results revealed that **BUC-12** was an effective catalyst over a wide pH range from 2.0 to 10.0, as illustrated in Fig. 7a. In order to investigate the activities of the organic ligands as photocatalysts, free L and phen were utilized to conduct MB degradation. Free L showed no photocatalytic activity, while phen was slightly soluble in water, and reacted stoichiometrically with MB under the experimental conditions, rather than acting as a photocatalyst. Also, tap water was used to prepare a MB solution in order to study the influence of dissolved salts on the photocatalytic MB decomposition. The photocatalytic degradation efficiency was inhibited by the total salts in water, as illustrated in Fig. 7b. The effects of individual cations and anions will be discussed in detail in our future work.

In order to test the practicability of these complexes as photocatalysts, **BUC-12** was selected to test the recyclability and stability by repeated runs in the photocatalytic degradation of MB under the usual reaction conditions. The results in Table 4 demonstrated that the photocatalytic performance remained almost unchanged after five runs, implying that **BUC-12** is stable under the catalytic

conditions. Furthermore, the PXRD diffraction patterns of the **BUC-12** after five runs again matched well with the simulated pattern generated from the single-crystal diffraction data, as shown in Fig. 8. Hence, **BUC-12** shows good reusability for the catalytic degradation of organic pollutants.

Conclusions

Four coordination compounds were synthesized via the hydrothermal method and characterized using single-crystal X-ray diffraction analysis, FTIR, UV–Vis DSR and CHN elemental analysis. The crystal structure analyses revealed that the supramolecular frameworks of **BUC-10**, **BUC-11**, **BUC-12** and **BUC-13** are constructed from discrete zero-dimensional units and lattice molecules via intermolecular hydrogen-bonding interactions. All of the complexes exhibited photocatalytic activities to decompose MB under UV light irradiation, implying their potential application as solid photocatalytic materials.

Supplementary materials

CCDC 1042968, 1042981, 1042975 and 1042979 contain the supplementary crystallographic data for compounds **BUC-10**, **BUC-11**, **BUC-12** and **BUC-13**. These data can be obtained free of charge from The Cambridge Crystallographic Data Centre via www.ccdc.cam.ac.uk/data_request/cif.

Acknowledgements We thank the financial support from National Natural Science Foundation of China (51578034), the Beijing Natural Science Foundation and Scientific Research Key Program of Beijing Municipal Commission of Education (KZ201410016018), the Importation & Development of High-Caliber Talents Project of Beijing Municipal Institutions (CIT&CD201404076), and Hundred, Thousand and Ten Thousand Talent Project of Beijing (2016023).

References

1. Wang C-C, Ho Y-S (2016) Research trend of metal–organic frameworks: a bibliometric analysis. Scientometrics 109(1):481–513
2. Hasegawa S, Horike S, Matsuda R, Furukawa S, Mochizuki K, Kinoshita Y, Kitagawa S (2007) Three-dimensional porous coordination polymer functionalized with amide groups based on tridentate ligand: selective sorption and catalysis. J Am Chem Soc 129(9):2607–2614
3. Wen T, Zhang D-X, Liu J, Lin R, Zhang J (2013) A multifunctional helical Cu (I) coordination polymer with mechanochromic, sensing and photocatalytic properties. Chem Commun 49(50):5660–5662
4. Lee JY, Farha OK, Roberts J, Scheidt KA, Nguyen SBT, Hupp JT (2009) Metal-organic framework materials as catalysts. Chem Soc Rev 38(5):1450–1459
5. Ming CL, Li YH, Li GY, Cui GH (2014) Synthesis, crystal structures, luminescence and catalytic properties of three silver(I) coordination polymers with bis(imidazole) and benzenedicarboxylic acid ligands. Transition Met Chem 39(4):477–485. doi:10.1007/s11243-014-9822-0
6. Zhang Y-Q, Wang C-C, Zhu T, Wang P, Gao S-J (2015) Ultrahigh uptake and selective adsorption of organic dyes with a novel polyoxomolybdate-based organic–inorganic hybrid compound. RSC Adv 5(57):45688–45692
7. Kuppler RJ, Timmons DJ, Fang Q-R, Li J-R, Makal TA, Young MD, Yuan D, Zhao D, Zhuang W, Zhou H-C (2009) Potential applications of metal-organic frameworks. Coord Chem Rev 253(23):3042–3066
8. Caskey SR, Wong-Foy AG, Matzger AJ (2008) Dramatic tuning of carbon dioxide uptake via metal substitution in a coordination polymer with cylindrical pores. J Am Chem Soc 130(33):10870–10871
9. Wang C-C, Li H-Y, Guo G-L, Wang P (2013) Synthesis, characterization, and luminescent properties of a series of silver (I) complexes with organic carboxylic acid and 1, 3-bis (4-pyridyl) propane ligands. Transition Met Chem 38(3):275–282
10. Ming C-L, Hao Z-C, Yu B-Y, Van Hecke K, Cui G-H (2015) Synthesis, structures, and catalytic properties of three new metal-organic coordination polymers constructed from flexible benzimidazole-based and cis-1, 2-cyclohexanedicarboxylate synthons. J Inorg Organomet Polym Mater 25(3):559–568
11. Qin L, G-y Li, Zheng J, S-l Xiao, G-h Cui (2013) Two 3D supramolecular architectures from Ag (I) coordination polymers constructed by flexible bis (benzimidazolyl) butane ligand. J Inorg Organomet Polym Mater 23(6):1266–1273
12. Wang S, Wang X (2015) Multifunctional metal–organic frameworks for photocatalysis. Small 11(26):3097–3112
13. Lee J, Farha OK, Roberts J, Scheidt KA, Nguyen ST, Hupp JT (2009) Metal–organic framework materials as catalysts. Chem Soc Rev 38(5):1450–1459
14. Jing H-P, Wang C-C, Zhang Y-W, Wang P, Li R (2014) Photocatalytic degradation of methylene blue in ZIF-8. RSC Adv 4(97):54454–54462
15. Wang C-C, Zhang Y-Q, Li J, Wang P (2015) Photocatalytic CO_2 reduction in metal–organic frameworks: a mini review. J Mol Struct 1083:127–136
16. Fu Y, Sun D, Chen Y, Huang R, Ding Z, Fu X, Li Z (2012) An amine-functionalized titanium metal–organic framework photocatalyst with visible-light-induced activity for CO_2 reduction. Angew Chem 124(14):3420–3423
17. Wang CC, Du XD, Li J, Guo XX, Wang P, Zhang J (2016) Photocatalytic Cr(VI) reduction in metal-organic frameworks: a mini-review. Appl Catal B Environ 193:198–216
18. Shen L, Liang R, Luo M, Jing F, Wu L (2014) Electronic effects of ligand substitution on metal-organic framework photocatalysts: the case study of UiO-66. Phys Chem Chem Phys 17(1):117–121
19. Lin H, Maggard PA (2008) Synthesis and structures of a new series of silver-vanadate hybrid solids and their optical and photocatalytic properties. Inorg Chem 47(18):8044–8052
20. Toyao T, Saito M, Horiuchi Y, Mochizuki K, Iwata M, Higashimura H, Matsuoka M (2013) Efficient hydrogen production and photocatalytic reduction of nitrobenzene over visible-light-responsive metal-organic framework photocatalyst. Catal Sci Technol 3(26):2092–2097
21. Liao Z-L, Li G-D, Bi M-H, Chen J-S (2008) Preparation, structures, and photocatalytic properties of three new uranyl– organic assembly compounds. Inorg Chem 47(11):4844–4853
22. Wang C-C, Zhang Y-Q, Zhu T, Zhang X-Y, Wang P, Gao S-J (2015) Four coordination compounds constructed from 1,10-phenanthroline and semi-flexible and flexible carboxylic acids:

hydrothermal synthesis, optical properties and photocatalytic performance. Polyhedron 90:58–68
23. Wang C-C, Wang P, Guo G-L (2012) 3D sandwich-like frameworks constructed from silver chains: synthesis and crystal structures of six silver (I) coordination complexes. Transition Met Chem 37(4):345–359
24. Zhang J, Wang C-C, Wang P, Gao S-J (2015) Three silver complexes constructed from organic carboxylic acid and 1,2-bis(4-pyridyl)ethane ligands: syntheses, crystal structures and luminescent properties. Transition Met Chem 40(8):821–829
25. Ye B-H, Tong M-L, Chen X-M (2005) Metal–organic molecular architectures with 2, 2′-bipyridyl-like and carboxylate ligands. Coord Chem Rev 249(5):545–565
26. Sen R, Mal D, Brandão P, Ferreira RAS, Lin Z (2013) Cadmium-furandicarboxylate coordination polymers prepared with different types of pyridyl linkers: synthesis, divergent dimensionalities, and luminescence study. Cryst Growth Des 13(12):5272–5281
27. Bruker AXS (2000) SMART, Version 5.611, Bruker AXS, Madison, WI, USA
28. Bruker AXS (2003) SAINT, Version 6.28, Bruker AXS, Madison, WI, USA
29. SADABS, V2.03 (2000) Bruker AXS, Madison, WI
30. Sheldrick GM (1997) SHELX-97. Göttingen University, Germany
31. Ma BQ, Gao S, Yi T, Yan CH, Xu GX (2000) A dimer structure [Cu(phen) 2 Cl][OH]·6H 2 O 2 constructed through C–H···Cl hydrogen bondings and π–π interactions. Inorg Chem Commun 3(3):93–95
32. Ye MD, Xiao HP, Hu ML (2001) Chloro-bis(1,10-phenanthroline)copper(II) 5-nitro-isophthalate(1 −) dihydrate. Acta Crystallogr 60(10):m1516–m1518
33. Zhang XJ, Ma TY, Yuan ZY (2008) Titania-phosphonate hybrid porous materials: preparation, photocatalytic activity and heavy metal ion adsorption. J Mater Chem 18(17):2003–2010
34. Hao JM, Yu BY, Hecke KV, Cui GH (2015) A series of d10 metal coordination polymers based on a flexible bis(2-methylbenzimidazole) ligand and different carboxylates: synthesis, structures, photoluminescence and catalytic properties. CrystEngComm 17(11):2279–2293
35. Ejhieh AN, Khorsandi M (2010) Photodecolorization of Eriochrome Black T using NiS–P zeolite as a heterogeneous catalyst. J Hazard Mater 176(1–3):629–637